Effect of transverse jet position on flame propagation regime

Wandong Zhao(赵万东)[1], Jianhan Liang(梁剑寒)[1], Ralf Deiterding[2], Xiaodong Cai(蔡晓东)[1,], Xinxin Wang(王鑫鑫)[1]*

1. Science and Technology on Scramjet Laboratory, College of Aerospace Science and Engineering, National University of Defense Technology, Changsha 410073, China

2. Aerodynamics and Flight Mechanics Research Group, University of Southampton, Boldrewood Innovation Campus, Southampton SO16 7QF, United Kingdom

Corresponding author,** ***Email:cai-chonger@hotmail.com **(*Xiaodong Cai*)**

ABSTRACT: *We studied the mechanisms of flame acceleration (FA) and deflagration to detonation transition (DDT) triggered by a combination of solid and jet obstacles. The Navier-Stokes equations with a detailed hydrogen-air kinetics model were utilized. Vast Kelvin-Helmholtz instabilities generate intensive turbulence-flame interactions, leading to an increase of surface area and high propagation velocity. The jet position has a significant effect on the FA and DDT. A choking flame and detonation flame are obtained by the transverse jet with different positions and mixing times even though in a lower blockage ratio.*

Direct ignition of the detonation combustion within a confined tube usually requires a high energy deposition, which is several orders of magnitude higher than the energy required for low-energy ignition[1]. Hence, it is still a challenge to activate the onset of detonation by this approach. As such, obtaining the onset of detonation combustion typically counts on the flame acceleration (FA) and deflagration to detonation transition (DDT) which usually stem from a weak energy ignition[2]. However, a shorter run-up time of the DDT is still a challenge, especially for a pulse detonation engine (PDE) with a high working frequency[3].

A typical obstacle such as orifice, ring, and Shchelkin spiral is adopted to stimulate the FA[4, 5]. The contributions of these obstacles are to introduce a suitable blockage ratio, perturb the flow, and provide a surface that reflects the compression and shock waves. As a result, the leading shock wave is generated subsequently, preheating the unburnt mixture[6]. Then the onset of detonation could be generated accordingly due to the hot spots caused by the shock convergence or energy deposition[4]. Tremendous efforts have been made to understand the performance and mechanisms in the FA introduced by solid obstacles[6-9]. The past studies reported that the flame can be accelerated from laminar flame to subsonic flame and even quench. The different flame propagation models can be observed in experimental results: quenching, choking, quasi-detonation, and detonation regimes[10-12]. For the choking flame, the propagation velocity of the flame usually travels at a speed around the local sound speed of the combustion products, meaning the failure of DDT because of the flame front decoupling from the leading shock, and the propagation velocity is near 1/3 to 1/2 of the theoretical Chapman–Jouguet (CJ) velocity[13]. But this propagation regime usually occurs in an obstacle-laden chamber with a high blockage ratio. This combustion regime is, however, not conducive for the PDE. In addition, many solid obstacles would result in a considerable pressure loss and around 25% thrust loss for a PDE as reported by Refs.[3, 14]. Recently, the transverse fluid obstacle, ejected into the smooth tube, is proposed as it can provide a suitable blockage ratio and also produce turbulent flows. Knox et al.[15] studied the composition of jet obstacles and demonstrated that the jet can also act as a virtual solid obstacle with lower pressure loss. Then, McGarry

et al.[16] revealed that the jet is more effective in converting laminar flame into fast-propagating turbulent flame. Several studies[17-19] have also proved that the jet obstacle is beneficial to shorten the time and required length of the DDT.

However, the effect of the jet position in the chamber on the FA and DDT processes is not clearly reported. Is there a suitable jet position for the onset of detonation, and is the ignition mechanism of detonation unchanged? Moreover, are arrangements with different jet positions equally beneficial for shorting the run-up distance of the DDT? Therefore, in this letter presented here, a combination of jet and solid obstacles is proposed, and the effect of the single jet with different positions in the obstacle-laden chamber on the FA and DDT is investigated in detail. Different propagation regimes such as the choking and detonation flames are observed, and the mechanisms of the choking flame and detonating ignition are revealed.

In this work, the codes solve the two-dimensional Naiver-Stokes equations associated with a reactive chemical source term for the FA and DDT processes. The equations were solved in the open-source programming of AMROC (Adaptive Mesh Refinement Object-oriented C++)[20], which has been successfully adopted previously in multi-dimensional detonation simulation, FA, and DDT[18, 21-23]. A Hybrid Roe-HLL Riemann solver was employed for discretizing the upwind scheme. The Minmod limiter with MUSCL reconstruction was utilized to construct a second-order accuracy in space. A semi-implicit generalized Runge-Kutta scheme with fourth-order accuracy was employed for the integration of chemical kinetics, which had been comprehensively validated by Deiterding's work[20]. The diffusion terms were discretized with second-order central differences. A level-set function with coupling to the ghost fluid method was adopted to implement the solid wall boundary[24]. The chemical reaction was modeled by a detailed 12 species 42 steps Arrhenius kinetic of the hydrogen-air mixture.

A typical configuration for the FA and DDT processes is illustrated in Fig. 1. Several rectangular solid obstructions are arranged within the tube with a size of $Lx \times Ly$=700 mm × 20 mm. A stoichiometric hydrogen-air mixture is used to fill the chamber. The parameters of the mixture are illustrated in Table 1, including the calculated properties such as the laminar flame thickness X_l, flame speed S_l, and several parameters after detonation, which are computed using Cantera[25].

FIG. 1. Schematic illustration of the combustion tube equipped with a combination of fluid and solid obstacles.

The mixture is ignited by a half-circle hot spot (r=4 mm) with a high temperature, T=2500 K, and it is located at the center of the left boundary. A low-pressure P=0.1 MPa is implemented to prevent a high flame propagation velocity (U_f) and shock wave formation at the initial stage. Ten pairs of solid obstructions are arranged in the upper and lower walls, corresponding to O(1), O(2), O(3), …, O(10), respectively. A large spatial interval of the solid obstacles is chosen with S=50 mm, so as to generate a Mach stem easily as reported by Ref.[6]. The width and height of the obstacle are set as d=2 mm, h=3 mm, respectively, producing a blockage ratio (Br) as Br=0.3. The distance L *is* 49 mm.

Table 1. The thermodynamics of hydrogen-air mixture and the corresponding parameters at CJ state.

Quantity	Value	Definition
P_0	0.1 MPa	Initial pressure

T_0	298 K	Initial temperature
M	21 g/mol	Molecular weight
S_l	≈0.298 m/s	Laminar flame speed
X_l	≈0.00035 m	Laminar flame thickness
P_{CJ}	15.58 P_0	CJ pressure
T_{CJ}	9.885 T_0	CJ temperature
ρ_{CJ}	1.52 kg/m^3	CJ density
V_{CJ}	1965 m/s	CJ speed
X_d	0.001-0.002 m	Cell width

All walls are set as adiabatic and no-slip boundary conditions, and the outflow boundary condition is assumed on the right. To trigger the FA, a combination of solid and transverse jet obstacles is proposed here so that one solid obstruction is replaced by a jet as illustrated in Fig. 1. Three different positions of the single jet are located at X_j=2.5, X_j=5, and X_j=7.5, corresponding to Case 1, 2 and 3. Note that the position of the jet is nondimensionalized by the width of the tube with $X_j=L_{jet}/Ly$. The width of the jet is also kept the same value as for the solid obstacle, and the pressure inlet boundary condition is adopted for the jet. The temperature and stagnation pressure of the jet equal T_{jet}=298 K and P_{jet}=0.35 MPa, respectively. The delay time of the jet is t=0.001 ms.

A mesh-resolution test is carried out firstly. The initial mesh width is set as $dx=dy=4.0\times10^{-4}$ m. The adaptive mesh refinement (AMR) technique is utilized so that it enables us to conduct a high-resolution simulation. Three different refinement stages are employed here, corresponding to Level 3 (refined uniformly by the successive factors 2, 2), 4 (2, 2, 2), and 5 (2, 2, 2, 2), exerting a refined mesh size of 1.0×10^{-4} m, 5.0×10^{-5} m, and 2.5×10^{-5} m. Therefore, the three cases result in 3.5, 7, and 14 grid cells within the laminar flame thickness. The test cases are run for the chamber with solid obstacles configuration and marginally high ignition energy (T=2500 K and P=0.6 MPa) is utilized throughout. The flame front propagation is superimposed in Fig. 2. The propagation of the flame tip in Level 4 and 5 is almost collapsed into one; therefore, the Level 4 setup is enough to cope with the FA. These results are coincident with the previous finding that a mesh with 5-10 cells per laminar thickness is accurate to resolve the FA and DDT[6, 13, 18, 26]. The operations of the AMR are unproblematic when there are high density and temperature gradients. The validation of the AMR criterion is ensured in our previous studies[18, 21]. Consequently, the Level 4 setup is employed in this engineering simulation considering the computing cost and accuracy. All Cases were run on the Tianhe-1 supercomputer, where 216 cores were employed, and every single case took around 13000 CPU×h.

The time sequence of the density and the subsequent temperature evolution in Case 1 is demonstrated in Fig. 3. The mixture is ignited and a wrinkled flame front is generated due to the flow instabilities[6]. The turbulent flow is observed owing to the transverse jet. At t=0.487 ms, a shrunken flame front is formed, proving that the jet also produces a suitable blockage ratio. Subsequently, the flame-turbulence interactions are observed, resulting in a long penetration length of the flame (Fig. 3(d)) due to the downstream vortexes. Such features increase the flame surface area dramatically and augment the energy release ratio[6], feeding back to increase the flame velocity U_f to a value as high as 700 m/s. Then the leading shock wave is formed thanks to compression wave convergence caused by the increasing ratio of the specific volume of the flame tip[27], preheating the fresh material. However, a splitting of the flame front is noted when the flame passes the obstructions from Fig. 3(h-j), presenting a conspicuous distortion of the flame front. This phenomenon is mainly a result of the flame-shock interactions, which generate an intensive Richtmyer–Meshkov

instability. Such feature leads to a gradual lengthening of the distance between the leading shock wave and flame front, L_{fs}. As a result, the DDT fails, which is called choking flame in Refs.[10, 13, 28].

FIG. 2. The propagation of flame front in three different refined levels.

FIG. 3. The evolution of temperature contours with flame propagation for Case 1.

Snapshots of temperature contour are presented in Figs. 4 and 5 for Case 2 and 3, respectively. Flame-turbulence interactions are observed (see Figs. 4(b) and 4(c)), resulting in a stretched flame front at t=0.912 ms. A strong leading shock wave is formed, so that shock-flame and shock-shock interactions occur in Figs. 4(e) and 4(f). The flame surface area increases dramatically thanks to the Kelvin-Helmholtz (K-H), Rayleigh-Taylor, and Richtmyer–Meshkov[29] instabilities when the reflected shock interacts with the flame tip. The temperature of the post-shock mixture is then increased. Additionally, a shock-flame complex is observed; therefore, L_{fs} is shorter than that in Case 1. Later, a local detonation has occurred and a remarkable detonation wave can be observed. Hence, the DDT is successful in Case 2. In terms of Case 3, the process can be summarized into four stages. First, the combustion flame propagates within the chamber, which is close to the previous study[1] that only has solid obstacles. The next stage is that of flame-turbulent interactions, leading to a high FA (see Figs. 5(c) and 5(d)). The third stage is the deflagration pattern, producing complicated shock-shock and shock-flame interactions where the large-scale turbulent flows, convoluted flame-turbulent and flame-shock interactions have occurred. The latter factors produce an environment very conducive for the formation of the DDT and detonation wave[30]. Last, the final stage is beginning with an established detonation from t=1.27822 ms.

FIG. 4. The evolution of temperature contour during the FA and DDT processes in Case 2.

FIG. 5. The snapshots of temperature contour during the FA and DDT processes in Case 3.

The propagation of the flame front and U_f for Case 1, 2, and 3 is plotted in Figs. 6(a) and 6(b), respectively. A higher speed is formed in Case 1 compared to Case 2 and 3 as proved by the circle in Fig. 6(b). However, the flame fronts in Case 2 and 3 catch up with that of Case 3 because of the DDT. Inflection points (see dashed and dotted circles in Case 2 and 3) are observed, respectively, caused by the occurrence of detonation. After an overdriven detonation, the U_f in both cases is close to a theoretical CJ value[31], demonstrating a highly accurate result in this study, whereas the required time and length of the DDT in Case 3 are both higher than that in Case 2. In terms of Case 1, a gradual decrease of U_f is observed. Therefore, the maximum flame velocity declines below the half CJ value, leading to the failure of transition. These results therefore indicate that the jet position has a significant effect on the DDT process. A jet with a much shorter or longer position has a negative effect on the DDT and even causes the transition to fail.

FIG. 6. (a) Flame position and (b) the propagation velocity of frame front variation over time for three cases.

To reveal these phenomena, the mechanisms of the successful and unsuccessful DDT can be explained as follows. The plots of U_f and L_{fs} versus the axial position are given by Figs. 7(a) and 7(b) for Case 1, respectively. A high fluctuation of U_f and L_{fs} occurs because of the solid obstruction, as shown in X=30 cm, 40 cm and 45 cm (ellipses A, B, and C), that generates a blockage first, then accelerates the flame. The maximum value of U_f first increases then decreases (see line A in Fig. 7(a)), resulting in a gradual decrease of the minimum velocity (see line B in Fig. 7(a)). This also leads to a gradually increasing length L_{fs} (see Fig. 7(b)). Finally, the velocity U_f is far away from the half CJ value, leading to the failure of DDT. The former study[28] suggested that the mechanism of the choking regime is governed by the gas dynamic jetting and not determined by the turbulent combustion. The results from Veser et al.[32] demonstrated that the flow behind the flame front is chocked when the flow speed of the products reaches the local sound speed, so that any pressure perturbation cannot contribute to increasing the flame surface area. Gamezo et al.[13] observed supersonic flows of the products, that travel at almost local sound speed, and found no evidence of the actual gas dynamic choking, but the flame regime is that of a quasi-detonation in the next propagation stage. To better reveal this choking flame, the temperature, pressure, local sound speed, and the corresponding Mach number are given in Fig. 8. It can be observed that there is a high-pressure region before the solid obstruction. The maximum Mach number of the products is close to 0.85, and the Mach number around the flame tip is close to 1.0, hence, there is still no choking of the products. The perturbations generating in the products, therefore, have not enough time to influence the leading edge of the flame surface and thereby the main mechanisms of the FA in the solid-laden chamber are disabled.

FIG. 7. (a) The flame propagation velocity and (b) the distance between the leading shock wave and flame front vary with the axial position in Case 1.

FIG. 8. The transient variations of temperature (upper row), pressure (second row), velocity (third row), and Mach number (lower row) contours.

The variations of the temperature in the downstream jet and nearby detonation ignition are given by Fig. 9 for Case 2. The corresponding vorticity and pressure contours are also presented. A stretched flame is formed (see rectangular regions denoted A1, A2 and B1), leading to the flame front passing the solid obstruction promptly. This is due to the pair vortexes (see rectangular regions C and D). Therefore, flame-vortex interactions are formed, increasing the flame surface area and leading to a high value of U_f. A high-pressure spot is generated (see rectangle F1) due to the reflected shock wave focusing, which couples with the flame front (see rectangle E1). Subsequently, a spherical detonation is triggered. Hence, the mechanism of detonation ignition in Case 2 is attributed to a high-pressure spot that couples with the flame front.

The flame propagation associated with Case 3 is demonstrated in Fig. 10. The flame front is squeezed when it passes the solid obstruction, as highlighted in point A1, which contributes to the interactions between the reflected wave and flame front, resulting in Richtmyer-Meshkov instabilities (see boxes B1 and B2). A curved flame front is also observed. A turbulent vortex is mainly responsible for this outcome, which can be made evident from the vorticity contours in

boxes C1, C2, and C3. Subsequently, the turbulent-flame interactions are formed. As a result, the flame front propagates with no apparent decrease as demonstrated by the velocity vectors.

Fig. 11 presents the density gradient. The jet leads to a remarkable appearance of K-H instabilities. When the jet impacts the upper wall, counterrotating turbulent structures are generated, which are called mushroom eddies[33, 34]. The clockwise and anticlockwise vortices are distorted, and the jet is deflected and slowly approaches the lower wall (Fig. 11(c)). Consequently, when the flame front approaches this region, the transverse jet is deflected, while larger uneven vortices are generated (Fig. 11(d)). This contributes to a gradually increasing pressure, making the transverse jet almost lose the function of blockage. However, the large vortices also wrinkle and stretch the flame front as demonstrated by the arrows in Fig. 11(e), yielding an increasing flame surface area. The shock wave and a wake of K-H instabilities from the tip of the obstacle can be observed in Fig. 11(g). The complicated reflected shock wave and the leading shock wave appear, forming a Mach stem in Fig. 11(h). Such features are also observed in Case 2. Finally, the local detonation is formed at the upper wall thanks to an energy deposition (see Fig. 11(i)).

FIG. 9. The snapshots of the flame propagation and the nearby detonation initiation (The contours are (a) temperature, (b) vorticity, (c) temperature, and (d) pressure from upper to lower row, respectively).

To better investigate the effect of the jet position on the FA, Fig. 12 plots the U_f variations along with the axial position for three cases. The profiles are almost collapsed into one at the initial time but vary in the next instant. Then Case 1 has a higher velocity U_f owing to an early turbulence-flame interaction (see region A). Further insight into these variations reveals that there are uniform augmentation regions in FA, occurring in the downstream jet as highlighted by regions A, B and C. Therefore, it can be concluded that the function of the transverse jet can be considered as a physical blockage object, and it also introduces a large part of turbulent flow and vortices, increasing the flame velocity significantly. Further, the augmentation region of the FA generated by the jet further results in a fast and stronger leading shock wave with a shorter length L_{fs} that is conducive for the DDT.

In this letter, the reactive Naiver-Stokes equations with an AMR technique were employed to simulate the FA and DDT processes. A combination of the jet and solid obstacles was proposed to stimulate the FA, and the effect of jet position on the FA and DDT processes was investigated in detail. The transverse jet has a significant influence on the FA, and not all fluid obstacles with different positions are conducive to the DDT. A stronger leading shock wave and shorter L_{fs} caused by the transverse jet due to the turbulent-flame interactions are beneficial for shortening the run-up time and distance of DDT. Whereas, when the flame propagation velocity is high enough and close to the local sound speed of the products, the later turbulent-flame interactions generated by the transverse jet have not a remarkable performance to shorten the time and length of the onset of detonation. Moreover, this study also demonstrates that the transverse jet with different positions and mixing times can be used to control the occurrence of DDT in a certain range. A single transverse jet would lead to some asymmetric effect on the FA so that the effect of the asymmetric pair of the solid obstacles on the FA should also be further investigated.

FIG. 10. Variations of the flame propagation (The contours are (a) temperature, (b) pressure, (c) vorticity, and (d) vector (the background is the density contour) from upper to lower row, respectively) for Case 3.

FIG. 11. The evolution of density gradient contour in Case 3.

FIG. 12. The flame front velocity varies along with the axial position for three cases.

ACKNOWLEDGMENTS

This work was supported by the National Natural Science Foundation of China (Nos. 11522222 and 91741205) and the China Scholarship Council (No. 202106110005).

DATA AVAILABILITY

The data that support the findings of this study are available from the corresponding author upon reasonable request.

CONFLICT OF INTEREST

The authors have no conflicts to disclose.

REFERENCES

1. E. S. Oran, G. Chamberlain, andA. Pekalski, "Mechanisms and occurrence of detonations in vapor cloud explosions," Progress in Energy and Combustion Science **77**, 100804 (2020).
2. C. M. Dion, D. M. Valiev, V. y. Akkerman, B. Demirgok, O. J. Ugarte, L.-E. Eriksson, andV. Bychkov, "Dynamics of flame extinction in narrow channels with cold walls: Heat loss vs acceleration," Physics of Fluids **33**, 033610 (2021).
3. G. D. Roy, S. M. Frolov, A. A. Borisov, andD. W. Netzer, "Pulse detonation propulsion: challenges, current status, and future perspective," Progress in Energy and Combustion Science **30**, 545 (2004).
4. G. Ciccarelli, andS. Dorofeev, "Flame acceleration and transition to detonation in ducts," Progress in energy and combustion science **34**, 499 (2008).
5. TaoLi, XiaohanWang, BaopengXu, andFanfuKong, "An efficient approach to achieve flame acceleration and transition to detonation," Physics of Fluids **33**, 056103 (2021).
6. V. N. Gamezo, T. Ogawa, andE. S. Oran, "Flame acceleration and DDT in channels with obstacles: Effect of obstacle spacing," Combustion and Flame **155**, 302 (2008).
7. V. N. Gamezo, C. L. Bachman, andE. S. Oran, "Flame acceleration and DDT in large-scale obstructed channels filled with methane-air mixtures," Proceedings of the Combustion Institute (2020).
8. G. B. Goodwin, R. W. Houim, andE. S. Oran, "Effect of decreasing blockage ratio on DDT in small channels with obstacles," Combustion and Flame **173**, 16 (2016).
9. V. y. Akkerman, andD. Valiev, "Moderation of flame acceleration in obstructed cylindrical pipes due to gas compression," Physics of Fluids **30**, 106101 (2018).
10. J. H. S. Lee, R. Knystautas, andC. K. Chan, "Turbulent flame propagation in obstacle-filled tubes," Symposium on Combustion **20**, 1663 (1985).
11. O. Peraldi, R. Knystautas, andJ. Lee, *Criteria for transition to detonation in tubes* (Elsevier, 1988).
12. J. Karnesky, E. Anderson, F. Schauer, andJ. Hoke, *Pulsed Detonation Engines in the Choked Flame Regime* (2012).
13. V. N. Gamezo, T. Ogawa, andE. S. Oran, "Numerical simulations of flame propagation and DDT in obstructed channels filled with hydrogen–air mixture," Proceedings of the Combustion Institute **31**, 2463 (2007).
14. M. Cooper, S. Jackson, J. Austin, E. Wintenberger, andJ. Shepherd, "Direct experimental impulse measurements for detonations and deflagrations," Journal of propulsion and power **18**, 1033 (2002).
15. B. W. Knox, D. J. Forliti, C. A. Stevens, J. L. Hoke, andF. R. Schauer, "Unsteady flame speed control and deflagration-to-detonation transition enhancement using fluidic obstacles," 48th AIAA Aerospace Sciences Meeting Including the New Horizons Forum and Aerospace Exposition 1 (2010).
16. J. P. McGarry, andK. A. Ahmed, "Flame–turbulence interaction of laminar premixed deflagrated flames," Combustion and Flame **176**, 439 (2017).
17. S. M. Frolov, V. A. Smetanyuk, V. S. Aksenov, andA. S. Koval', "Deflagration-to-detonation transition in crossed-flow fast jets of propellant components," Doklady Physical Chemistry **476**, 153 (2017).
18. H. Peng, Y. Huang, R. Deiterding, Z. Luan, F. Xing, andY. You, "Effects of jet in crossflow on flame acceleration and deflagration to detonation transition in methane–oxygen mixture," Combustion and Flame **198**, 69 (2018).
19. J. Cheng, B. Zhang, H. Liu, andF. Wang, "The precursor shock wave and flame propagation enhancement by CO2 injection in a methane-oxygen mixture," Fuel **283**, (2021).
20. R. Deiterding, *Parallel adaptive simulation of multi-dimensional detonation structures* (Dissertation. de, 2003).
21. X. Cai, R. Deiterding, J. Liang, M. Sun, andY. Mahmoudi, "Diffusion and mixing effects in hot jet initiation and propagation of hydrogen detonations," Journal of Fluid Mechanics **836**, 324 (2018).
22. H. Wei, X. Zhang, H. Zeng, R. Deiterding, J. Pan, andL. Zhou, "Mechanism of end-gas autoignition induced by flame-pressure interactions in confined space," Physics of Fluids **31**, (2019).
23. W. Chen, J. Liang, X. Cai, andY. Mahmoudi, "Three-dimensional simulations of detonation propagation in circular tubes: Effects of jet initiation and wall reflection," Physics of Fluids **32**, 046104 (2020).
24. R. Deiterding, "A parallel adaptive method for simulating shock-induced combustion with detailed chemical kinetics in complex domains," Computers & Structures **87**, 769 (2009).
25. D. G. Goodwin, H. K. Moffat, andR. L. Speth, "Cantera: An object-oriented software toolkit for chemical kinetics, thermodynamics, and transport processes," Caltech, Pasadena, CA (2009).
26. D. Kessler, V. Gamezo, andE. Oran, "Simulations of flame acceleration and deflagration-to-detonation transitions in methane–air systems," Combustion and Flame **157**, 2063 (2010).
27. Vasilyev, Oleg, V., Aslani, Mohamad, Kassoy, David, R., Regele, andJonathan, "Evolution of detonation formation initiated by a spatially distributed, transient energy source," Journal of Fluid Mechanics (2016).
28. J. Chao, andJ. H. S. Lee, "The propagation mechanism of high speed turbulent deflagrations," Shock Waves **12**, 277 (2003).
29. M. Bambauer, N. Chakraborty, M. Klein, andJ. Hasslberger, "Vortex dynamics and fractal structures in reactive and nonreactive Richtmyer–Meshkov instability," Physics of Fluids **33**, 044114 (2021).

30. O. Y. Al-Thehabey, "Modeling the amplitude growth of Richtmyer–Meshkov instability in shock–flame interactions," Physics of Fluids **32**, 104103 (2020).
31. J. H. Lee, *The detonation phenomenon* (2008).
32. A. Veser, W. Breitung, andS. B. Dorofeev, "Run-up distances to supersonic flames in obstacle-laden tubes," Journal De Physique IV **12**, 333 (2002).
33. D. J. Tarrant, J. Chambers, andK. A. Ahmed, *Fast Flame Interaction with High Pressure Turbulent Jets for Turbulent Deflagration-to-Detonation Transition* (2018).
34. R. F. Huang, andJ. Lan, "Characteristic modes and evolution processes of shear-layer vortices in an elevated transverse jet," Physics of Fluids **17**, 034103 (2005).

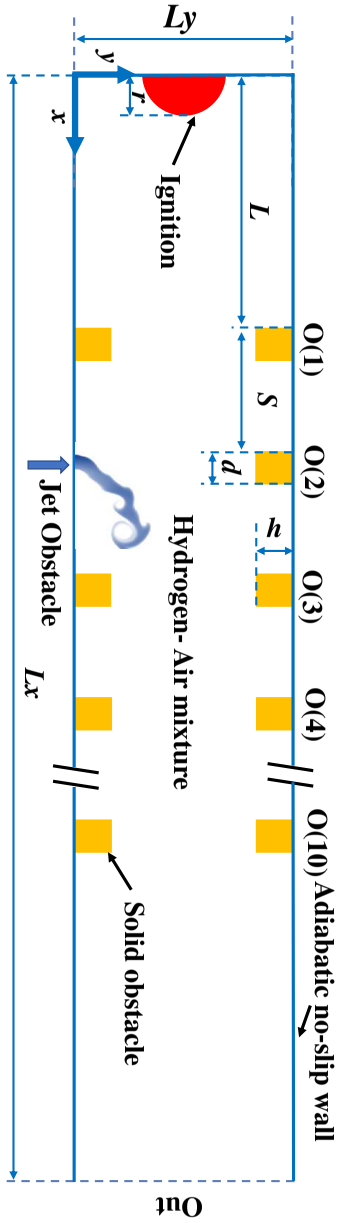

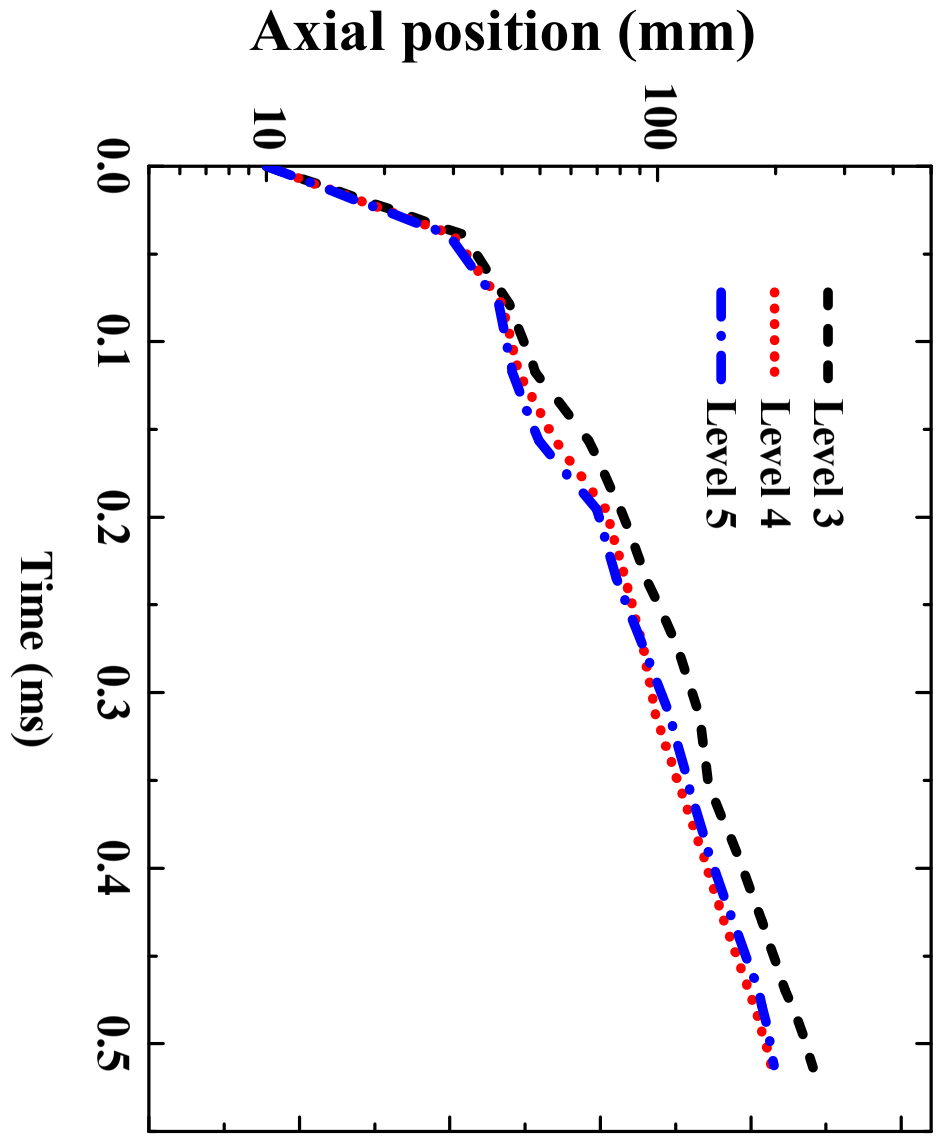

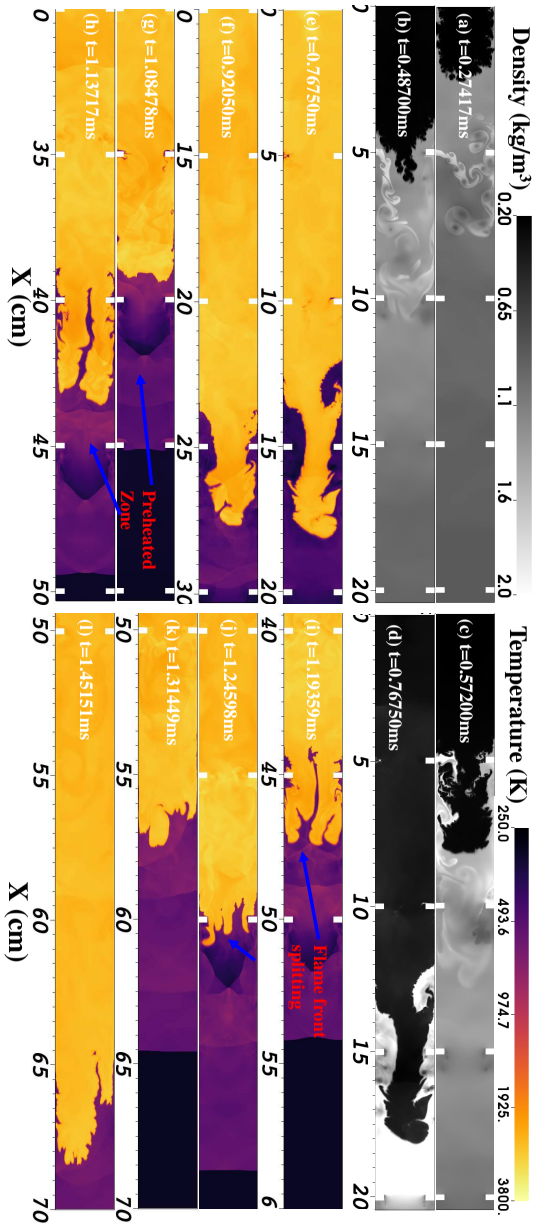

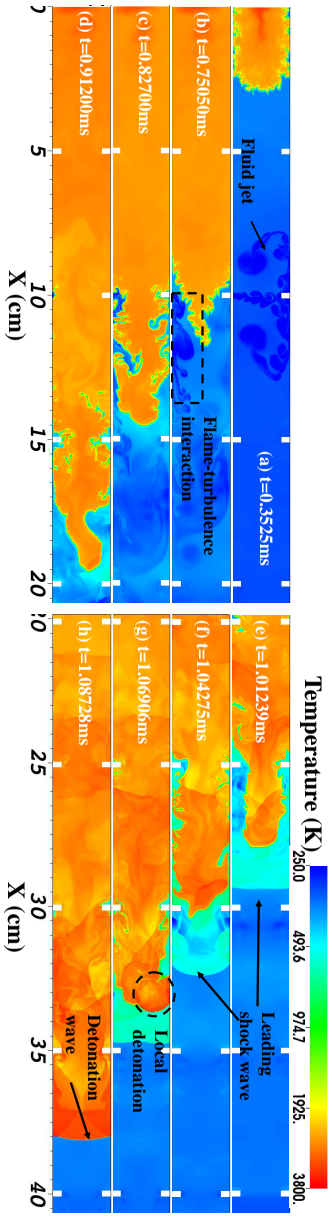

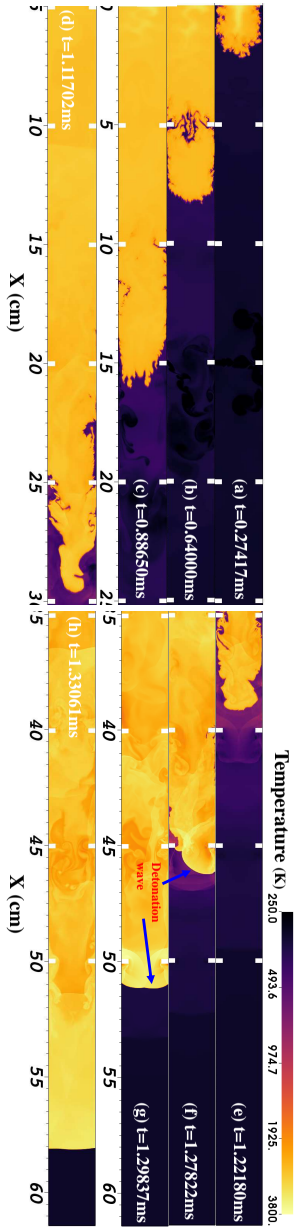

PLEASE CITE THIS ARTICLE AS DOI: 10.1063/5.0063363